

# Strongly anharmonic collective modes in a coupled electron-phonon-spin problem

Sauri Bhattacharyya<sup>1</sup>, Sankha Subhra Bakshi<sup>1</sup>, Saurabh Pradhan<sup>2</sup> and Pinaki Majumdar<sup>1</sup>

<sup>1</sup> Harish-Chandra Research Institute, HBNI, Chhatnag Road, Jhansi, Allahabad 211 019, India

<sup>2</sup> Department of Physics and Astronomy, Uppsala University, 751 05 Uppsala, Sweden

(Dated: December 18, 2019)

We solve for the finite temperature collective mode dynamics in the Holstein-double exchange problem, using coupled Langevin equations for the phonon and spin variables. We present results in a strongly anharmonic regime, close to a polaronic instability. For our parameter choice the system transits from an ‘undistorted’ ferromagnetic metal at low temperature to a structurally distorted paramagnetic insulator at high temperature, through a short range charge ordered (CO) phase near the ferromagnetic crossover at  $T_{FM}$ . The small amplitude harmonic phonons at low temperature cross over to large amplitude dynamics around  $0.5T_{FM}$  due to thermally generated short range correlated polarons. The rare thermal “tunneling” of CO domains generates a hitherto unknown momentum selective spectral weight at very low energy. We compare our results to inelastic neutron data in the manganites and suggest how the singular low energy features can be probed.

Collective modes play a crucial role in dictating low-energy spectral and transport properties in correlated electron systems [1–3]. The most detailed information about them comes from inelastic neutron scattering (INS) experiments [4–18], which probe the momentum resolved spectrum of lattice, magnetic, or density fluctuations. The interpretation of INS results has depended, traditionally, on schemes like the random phase approximation (RPA), for phonons, or the  $1/S$  expansion for spins. These methods are meant to access low amplitude fluctuations and are limited to low temperature.

Correlated electron systems often show thermal phase transitions, or strong short range correlated distortions [1–3], where the low temperature ‘linearised’ dynamics is no longer useful in describing the modes. While methods like time dependent Ginzburg-Landau (TDGL) theory [19, 20] or full scale ‘molecular dynamics’ (MD) [21, 22] are available in classical systems, equivalent real time methods are rare in quantum systems. To address collective mode physics in these systems a method should handle the strong interactions reliably, capture large dynamical fluctuations in real time, be sensitive to spatial correlations, and access finite temperature.

In this paper we demonstrate a ‘real space’, real time method that probes the dynamics of phonons and spins strongly coupled to an electron system, handles strong interactions non perturbatively, and accesses thermal physics. We deliberately choose an ‘operating point’ where anharmonic effects in the phonons - arising from mode coupling, polaron ‘tunneling’, and magnetic fluctuations - are large. This allows us to demonstrate the uniqueness of the method, and also address dynamics in the manganites as a non trivial test case.

The manganites provide a concrete template for thermally induced anharmonic fluctuations. The itinerant  $e_g$  electrons in these materials are strongly coupled to lattice modes via Jahn-Teller (JT) coupling [2], and to  $t_{2g}$  based core spins via large Hund’s coupling [2, 23]. The JT coupling favours polaron formation (and electron localisation), while the Hund’s coupling favours a ferromagnetic metallic (FM-M) state. There are materials, *e.g.*,  $\text{La}_{1-x}\text{Ca}_x\text{MnO}_3$ , with  $x \sim 0.3$ , where thermally induced polaronic distortions convert a homogeneous low  $T$  FM-M to a structurally distorted polaronic insulator above

magnetic transition at  $T_{FM}$ . The structural and transport features of this problem [2, 24–30] has seen much analysis [31–33] over the last two decades while the thermal dynamics remained virtually unaddressed.

Experiments exist on the phonon [6–9] and spin dynamics [12–18]. INS results reveal that (i) in  $\text{La}_{1-x}\text{Sr}_x\text{MnO}_3$  with  $x \sim 0.2 - 0.3$ , the transverse acoustic phonons show anomalous softening and broadening [6, 7] on heating through  $T_{FM}$ , while (ii) the magnons along (100) and (110) directions in  $\text{La}_{0.7}\text{Ca}_{0.3}\text{MnO}_3$  [12, 15, 18] and  $\text{La}_{0.8}\text{Sr}_{0.2}\text{MnO}_3$  [13, 16] show large linewidths and softening near  $T_{FM}$ , which can’t be explained using a simple spin model.

Our work reveals that for a model that involves thermally induced metal-insulator transition via polaron formation, the dynamical features above arise naturally, and, additionally, are accompanied by rare events relating to polaron tunneling. This leads to a remarkable low energy signature in the spectrum. We use a Langevin dynamics approach [34, 35], new to these problems, a Holstein model, rather than Jahn-Teller, for the phonons, a large Hund’s coupling to drive ferromagnetism, and solve a two dimensional [36] electron problem. The electron-phonon (EP) coupling is chosen so that the  $T = 0$  system is just below the polaronic instability. The bare phonon frequency is  $\Omega$ . Our main results are the following.

(A). *Phonons*: The phonon spectrum exhibits the expected ‘RPA’ dispersion at  $T = 0$ , with resolution limited lineshapes, but increasing  $T$  leads to three prominent effects: (a) The growing phonon distortions, and the associated electron density, order in a short range pattern with wavevector  $\mathbf{Q} \sim (\pi, \pi)$  and the phonon dispersion for momentum  $\mathbf{q} \sim \mathbf{Q}$  softens significantly. (b) The damping  $\Gamma_{\mathbf{q}}$  is strongest for  $\mathbf{q} \sim \mathbf{Q}$  and grows rapidly with  $T$  due to a combination of anharmonic phonon interaction and magnon-phonon coupling. (c) The short range correlated structures have their own slow dynamics - involving thermally assisted tunneling - and this generates visible spectral weight at frequency  $\omega \ll \Omega$  for  $\mathbf{q} \sim \mathbf{Q}$ .

(B). *Magnons*: The low temperature magnons are as expected in a ferromagnet, with  $\omega_s(\mathbf{q}) \sim J_{eff}(2 - \cos(q_x a) - \cos(q_y a))$ , where  $J_{eff} \sim 0.1t$ , and resolution limited widths. Temperature brings in two features: (a) the spectrum narrows

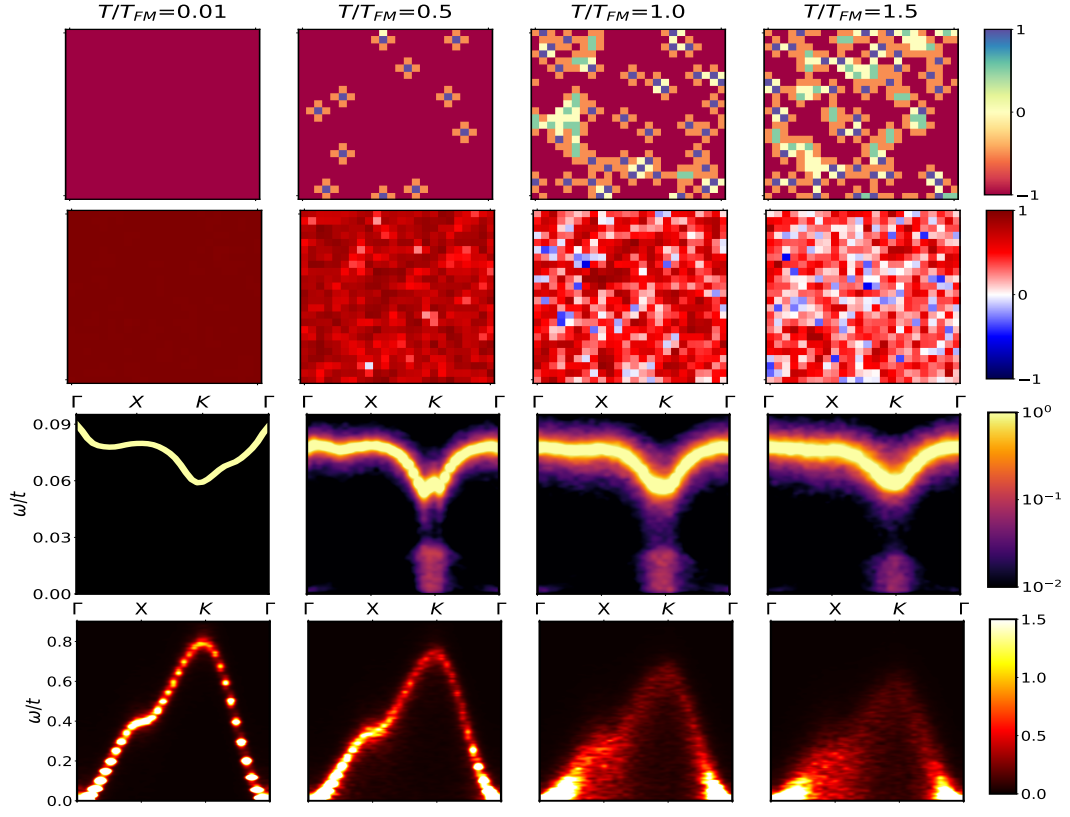


FIG. 1. Phonon and spin snapshots at temperatures  $T/T_{FM} = 0.01, 0.5, 1.0, 1.5$  and the corresponding spectral maps. The  $T$  are chosen to represent low, intermediate, ‘critical’, and high temperature regimes. First row: snapshot of the phonon field  $x_i(t)$ , showing the change from an undistorted low  $T$  state to a progressively large distortion checkerboard correlated state with temperature. Second row: snapshot of nearest-neighbour spin correlation:  $O_i(t) = \frac{1}{4} \sum_{\delta} \vec{S}_i(t) \cdot \vec{S}_{i+\delta}(t)$ , showing the evolution from a perfect FM to a disordered state on heating through  $T_{FM}$ . Third row: phonon power spectrum  $\frac{1}{T} |X(\mathbf{q}, \omega)|^2$  for  $\mathbf{q}$  varying along  $\Gamma - X - K - \Gamma$  in the Brillouin zone. We see a thermally induced softening and broadening for modes with  $\mathbf{q} \sim (\pi, \pi)$ , along with an unexpected  $\omega \rightarrow 0$  feature for  $T \gtrsim 0.5T_{FM}$ . Fourth row: magnon power spectrum  $\frac{1}{T} |S(\mathbf{q}, \omega)|^2$ , starting from a Heisenberg-like spectrum with  $J_{eff} \sim 0.1t$ , shows overall softening and large dampings near  $(\pi, 0)$  and  $(\pi, \pi)$  on heating up.

and the mean dispersion shows a softening that is roughly linear in  $T$ , and (b) The damping stays small till  $T \sim 0.5T_{FM}$  and then shows a dramatic increase. Unlike phonons, for whom the principal weight remains at  $\omega \sim \Omega$ , the high temperature magnon lineshape is very broad.

**Model and method:** We study the Holstein-double exchange (HDE) model on a two-dimensional square lattice.

$$H = -t \sum_{\langle ij \rangle} c_{i\sigma}^\dagger c_{j\sigma} - J_H \sum_i \vec{S}_i \cdot \vec{\sigma}_i - \mu \sum_i n_i - g \sum_i n_i x_i + \sum_i \left( \frac{p_i^2}{2M} + \frac{1}{2} K x_i^2 \right) \quad (1)$$

We study a nearest neighbour model with  $t = 1$  at density  $n = 0.40$ .  $K$  and  $M$  are the local stiffness and mass, respectively, of the optical phonons, and  $g = 1.40$  is the electron-phonon coupling. We set  $K = 1$ . In this paper, we report studies for  $\Omega = \sqrt{K/M} = 0.1t$ , which is a reasonable value for real materials.  $\vec{S}_i$ ’s are ‘core spins’, assumed to be large and classical. The chemical potential  $\mu$  is varied to maintain the

electron density at the required value. We work in the Hund’s coupling limit  $J_H/t \gg 1$ .

The thermal dynamics of the phonons and spins is solved using the coupled Langevin equations (see Supplement):

$$\begin{aligned} M \frac{d^2 x_i}{dt^2} &= -D_{ph} \frac{dx_i}{dt} - K x_i - \frac{\partial \langle H_{el} \rangle}{\partial x_i} + \xi_i(t) \\ \frac{d\vec{S}_i}{dt} &= -\vec{S}_i \times \left( \frac{\partial \langle H_{el} \rangle}{\partial \vec{S}_i} + \vec{h}_i \right) + D_s \vec{S}_i \times (\vec{S}_i \times \frac{\partial \langle H_{el} \rangle}{\partial \vec{S}_i}) \\ H_{el} &= \sum_{ij} (t_{ij} - \mu \delta_{ij}) \gamma_i^\dagger \gamma_j - g \sum_i n_i x_i \\ t_{ij}/t &= \sqrt{(1 + \vec{S}_i \cdot \vec{S}_j)/2} \end{aligned} \quad (2)$$

The phonon equation [35] involves inertia, damping, an effective force from the electronic energy, and noise. The noise satisfies the fluctuation-dissipation theorem (FDT) and is specified by  $\langle \xi_i(t) \rangle = 0$ ,  $\langle \xi_i(t) \xi_j(t') \rangle = 2D_{ph} k_B T \delta_{ij} \delta(t - t')$ . The spin dynamics follows a Landau-Lifshitz-Gilbert-Brown (LLGB) equation [37]. The first term on the right hand side of the spin equation is the torque and the second term is the

Gilbert damping. The noise  $\vec{h}_i$  also satisfies FDT but enters in a ‘multiplicative’ form, crossed with the spin field  $\vec{S}_i$  itself. The spin evolution conserves  $|\vec{S}_i|$ .

There are multiple timescales involved. We set the bare oscillation period for the phonons,  $\tau_{ph} = 2\pi/\Omega$ , as the unit of time. The low  $T$  relaxation time for phonons is  $2M/D_{ph} \sim 60\tau_{ph}$ , for  $D_{ph} = 0.05t$ . For magnons, the typical time period is set by  $\tau_s = 1/J_{eff}$  of the effective Heisenberg model, roughly  $10/t$ . The low  $T$  magnon relaxation timescale is  $D_s^{-1} \sim 4\tau_s$ . For our parameter choice  $\tau_{ph} \sim 6\tau_s$ . The largest timescale is for phonon relaxation, at  $60\tau_{ph}$ , and the smallest is for magnetic oscillations at  $\sim (1/6)\tau_{ph}$ . The numerical scheme has to use time discretisation and overall runtime keeping these in mind. The choice of  $D_{ph}$  and  $D_s$  is discussed in the Supplement.

The evolution equations are numerically integrated using the Euler-Maruyama [38] scheme for phonons and a Suzuki-Trotter decomposition based method [39] for spins. The time step is  $\Delta t = 1.6 \times 10^{-4}\tau_{ph}$ . We typically ran our simulations on systems of size  $24 \times 24$  for  $10^7$  steps, *i.e.*  $\sim 10^3\tau_{ph}$ . This ensured that we had enough time for equilibration and enough frequency resolution to compute the power spectrum.

**Results:** We organize the results in three parts: (a)  $T$  dependence of the typical instantaneous phonon and spin backgrounds and gross spectral features, (b) the phonon and magnon lineshape at a few momenta, and (c) comparison of our results with inelastic neutron data on the manganites.

Fig. 1 correlates the typical phonon and spin backgrounds, in the upper two rows, obtained as instantaneous Langevin configurations, with the momentum resolved power spectrum of the phonons and spins in the bottom two rows. The top row shows phonon configurations  $\{x_i\}$ . We see an undistorted state at low  $T$  (left panel) gradually forming patches of checkerboard ordered large distortions on heating up. These patches proliferate in the critical regime. The changing  $x_i$  background leads to a rise in the density correlation function  $S_n(\mathbf{q})$  at  $\mathbf{q} = (\pi, \pi)$ , shown in the Supplement. The second row shows snapshots of the nearest neighbour summed overlap  $O_i(t) = \frac{1}{4} \sum_{\delta} \vec{S}_i(t) \cdot \vec{S}_{i+\delta}(t)$ , which indicate a ferromagnetic low  $T$  state, and progressively spin disordered configurations on heating across  $T_{FM}$ . The  $T$  dependence of the associated FM peak,  $S_s(0, 0)$ , in the structure factor, is shown in the Supplement. The magnetic disorder aids lattice polaron formation by suppressing the hopping.

The third row shows  $\frac{1}{T} |X(\mathbf{q}, \omega)|^2$ , where  $X(\mathbf{q}, \omega) = \sum_i e^{i\mathbf{q} \cdot \mathbf{r}_i} \int dt e^{-i\omega t} x_i(t)$ . Sample behaviour of  $x_i(t)$  in different  $T$  regimes is shown in the Supplement. The low temperature phonon spectrum (first column) is accessible through a harmonic theory, equivalent to RPA in the quantum context, with intersite phonon correlations arising via the ‘bare’ electronic polarisability  $\Pi_0(\mathbf{q})$ . The phonon dispersion has a form  $\omega_{ph}^0(\mathbf{q}) \sim \sqrt{(K + g^2\Pi_0(\mathbf{q}))/M}$  and the damping  $\Gamma_{ph}(\mathbf{q})$  of these ‘normal modes’ is  $\sim D_{ph}/M$ . On heating up, the typical  $x_i$  increase in magnitude and the spectrum displays three distinct features- (i) increased damping due to anharmonicity induced coupling between normal modes, (ii) ‘softening’ of

the dispersion near  $\mathbf{q} = (\pi, \pi)$ , related to enhanced CO correlations, and (iii) the appearance of spectral weight at low frequencies,  $\omega \ll \Omega$ ! The low-energy feature arise from rare tunneling of checkerboard correlated patches that lead to large local ‘switching’ of the  $x_i$ . The low energy weight reduces when  $T \gg T_{FM}$  where large amplitude oscillations and tunneling events can no longer be distinguished. We will discuss the impact of the magnetic degrees of freedom on the phonons later in the paper.

The fourth row shows  $\frac{1}{T} |\vec{S}(\mathbf{q}, \omega)|^2$ , where  $\vec{S}(\mathbf{q}, \omega) = \sum_i e^{i\mathbf{q} \cdot \mathbf{r}_i} \int dt e^{-i\omega t} \vec{S}_i(t)$ . The low temperature spectrum corresponds to FM spin waves, with  $\omega_s^0(\mathbf{q}) \sim J_{eff}(2 - \cos(q_x a) - \cos(q_y a))$  and can be reproduced using a nearest neighbour FM Heisenberg model with  $J_{eff} \approx 0.1t$ . Increasing  $T$  reveals a suppression of the intensity and a slow increase in magnon damping. Beyond  $\sim 0.5T_{FM}$  the magnon lines broaden rapidly, notably near  $(\pi, 0)$  and  $(\pi, \pi)$ . Beyond  $T_{FM}$ , most of the modes are diffusive in nature, except near

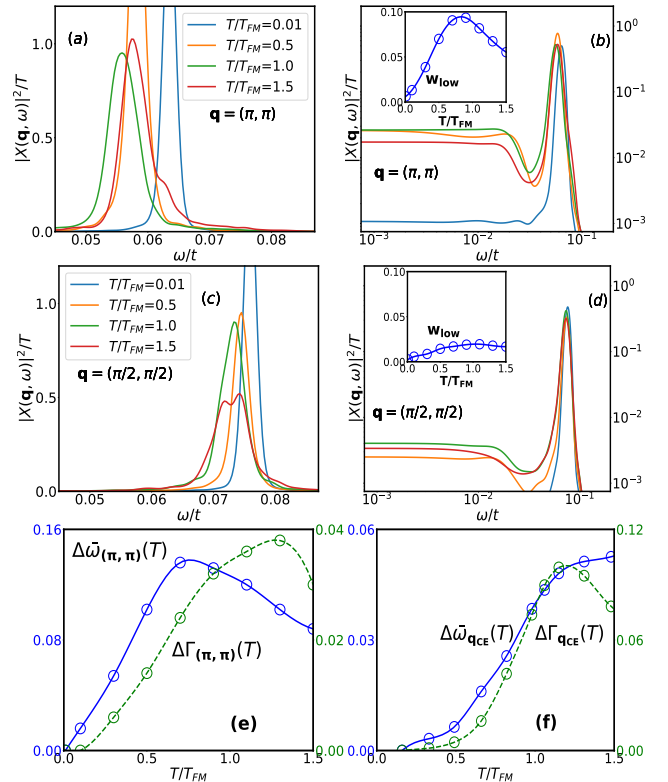


FIG. 2. Top row: Phonon lineshape for  $\mathbf{q} = (\pi, \pi)$  on a linear (a) and logarithmic (b) scale. The temperatures chosen are  $T/T_{FM} = 0.01, 0.5, 1.0, 1.5$ . We observe a  $\sim 15\%$  softening of mode frequency and a sharp increase in the linewidth with  $T$  in (a). The accumulation of low-energy weight is emphasized in (b), where the inset shows a detailed  $T$  dependence. Middle: the same analysis is repeated for  $\mathbf{q} = (\pi/2, \pi/2)$  in (c) and (d). Similar trends persist with much reduced extent. Bottom: Theoretically extracted ‘softening’  $\Delta\bar{\omega}_{(\pi,\pi)}(T) = \bar{\omega}_{(\pi,\pi)}(0) - \bar{\omega}_{(\pi,\pi)}(T)$  and thermal broadening  $\Delta\Gamma_{(\pi,\pi)}(T) = \Gamma_{(\pi,\pi)}(T) - \Gamma_{(\pi,\pi)}(0)$  in (e) is compared to corresponding quantities for  $\mathbf{q} = \mathbf{q}_{CE}$  from experiments (f). Qualitative trends are similar.

the zone center. These thermal trends are qualitatively similar to the Heisenberg model [40, 41] and also to a pure double exchange model at the same density. We will discuss the relative insensitivity of magnons to phonon physics later.

Fig.2 examines phonon lineshapes in detail at two momenta,  $\mathbf{q} = (\pi, \pi)$  and  $(\pi/2, \pi/2)$ . Panel 2(a) focuses on the ‘high energy’ part of the spectrum,  $\omega \sim \Omega$ , at  $\mathbf{q} = (\pi, \pi)$ , while 2(b) uses a logarithmic frequency and amplitude scale to show the full  $\mathbf{q} = (\pi, \pi)$  data. In 2(a), we see a striking enhancement of broadening in the high-energy part of the spectrum on heating from the  $T = 0.01T_{FM}$  to  $T \sim T_{FM}$ . A reduction of the mean frequency is also observed. To clarify the behaviour at  $\omega \ll \Omega$  panel 2(b) depicts the full spectrum in a log-log plot. This reveals the low frequency spectral weight arising from polaron tunneling. The inset shows the  $T$  dependence of the low frequency weight  $w_{low}(\mathbf{q}, T) = \int_0^{\Omega_{low}} d\omega |X(\mathbf{q}, \omega)|^2$ , normalised by the full weight. We use  $\Omega_{low} = 0.4\Omega$ . The weight  $w_{low}$  is non monotonic in  $T$  with a reasonable maximum value  $\sim 10\%$ . 2(c)-(d) repeats the same analysis for  $(\pi/2, \pi/2)$ , which is considerably separated from the ‘CO’ wavevector. The trends are similar to  $\mathbf{q} = (\pi, \pi)$  but the peak  $w_{low}$  is much smaller,  $\sim 3\%$ .

Figs.2(e) and 2(f) show a comparison of the softening and damping inferred from our  $(\pi, \pi)$  phonon lineshape with that extracted from experimental data at the ‘CE ordering’ wavevector  $\mathbf{q} = \mathbf{q}_{CE}$ . The experimental data is on *acoustic* phonons, but its has been argued that the behaviour should be similar to that of the JT phonons. Both theory and experimental results are normalised by the respective low  $T$  bandwidth, and temperatures are scaled by the respective  $T_{FM}$ ,  $\sim 0.1t$  in the model and 305K in experiments. The  $T$  dependence in panels (e) and (f) share similarities but actual numbers differ [42] by  $\sim$  a factor of 2. We discuss the comparison in more detail later. To the extent we know, experiments have not probed the low frequency part of the spectrum.

Figs.3 is focused on magnons, at  $\mathbf{q} = (\pi, 0)$  and  $(\pi, \pi)$ . The lineshapes show that the sharp dispersive feature for  $T \lesssim 0.5T_{FM}$  and then rapid broadening as  $T \rightarrow T_{FM}$ . The  $(\pi, 0)$  mode softens much less than the mode at  $(\pi, \pi)$ . In 3(c) and 3(d), the detailed temperature dependence of softening,  $\Delta\omega_{\mathbf{q}}(T)$ , and damping,  $\Delta\Gamma_{\mathbf{q}}(T)$ , are shown. The normalizing energy scale is the low  $T$  magnon bandwidth ( $\sim 0.8t$  in our case). We have not been able to find systematic temperature dependence data on magnon lineshapes in the manganites, although a body of results [12, 13, 15, 18] point out low temperature magnon ‘anomalies’ in these materials.

**Discussion:** Having presented the results, in what follows we provide an analysis of the features in Figs.1-3, and point out where our results match with, differ from, and go beyond measurements in the manganites.

We broadly observe four phonon regimes- (i) harmonic,  $\sim 0 - 0.1T_{FM}$ , (ii) anharmonic,  $\sim 0.1T_{FM} - 0.3T_{FM}$ , (iii) polaronic,  $\sim 0.3T_{FM} - 1.5T_{FM}$ , and (iv) large oscillations,  $\gtrsim 1.5T_{FM}$ , in terms of real-time dynamics (see Supplement for  $x_i(t)$  data). The harmonic to anharmonic crossover is reflected in the  $T$  dependence of  $\Gamma(\mathbf{q})$  due to mode cou-

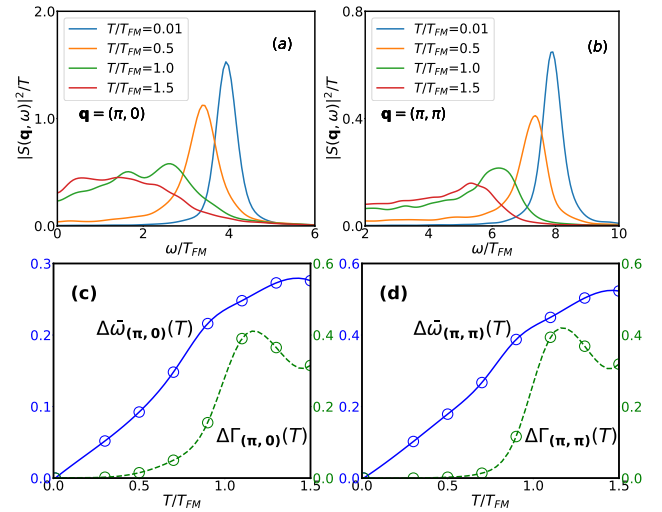


FIG. 3. Top panel: Magnon lineshapes for  $\mathbf{q} = (\pi, 0)$  (a) and  $\mathbf{q} = (\pi, \pi)$  (b) at the same temperatures. The low  $T$  spectrum is concordant with a nearest neighbour Heisenberg model for  $J_{eff} \sim 0.1t$ . Near  $T_{FM}$ , asymmetric and broad lineshapes are seen. Bottom: Theoretical estimates of ‘mode softening’ and broadening for magnons (similar to phonons) for  $(\pi, 0)$  (c) and  $(\pi, \pi)$  (d). We see enhanced softening in the latter.

pling. In the polaronic regime the distortions increase and we observe ‘burst like’ events - anticorrelated between nearest neighbour sites. For  $T \gtrsim 1.5T_{FM}$  the oscillations are even larger but the spatial correlations begin to weaken. Regimes (iii) and (iv) contain appreciable effect of magnetic disorder, which results in a peak in  $\Gamma_{ph}(\mathbf{q}, T)$  for  $T \sim T_{FM}$  for the present case - in contrast to a pure Holstein model.

The observed magnon spectra are similar to those of a nearest-neighbour Heisenberg model. The ‘square root’ renormalization of stiffness, and phonon couplings, are both seemingly irrelevant. There are broadly three magnon regimes- (i) free,  $\sim 0 - 0.5T_{FM}$ , (ii) interacting,  $\sim 0.5T_{FM} - T_{FM}$ , and (iii) diffusive,  $\gtrsim T_{FM}$ . The  $(1 + \langle S_i \cdot S_j \rangle)^{1/2}$  factor varies by  $\sim 15\%$  from  $0 - T_{FM}$ , while  $\langle \gamma_i^\dagger \gamma_j \rangle$  is almost  $T$  independent. Due to this an essentially phonon insensitive Heisenberg description arises. The overall picture holds even in presence of a *small*  $J_{AF}$ , whose main effect is bandwidth reduction at low  $T$ .

Our parameter choice was meant to mimic the physics in  $\text{La}_{1-x}\text{Sr}_x\text{MnO}_3$  and  $\text{La}_{1-x}\text{Ca}_x\text{MnO}_3$  for  $x \sim 0.2 - 0.3$ . Unlike the real material, the model we use is two dimensional, involves Holstein rather than cooperative JT phonons, and does not include AF couplings. As Figs.2(e)-(f) demonstrate the phonon softening at the short range ordering wavevector follows similar trends in theory and experiment roughly upto  $T_{FM}$ , beyond which they deviate. The fractional softening near  $T_{FM}$  however differs by more than a factor of two. Similarly, the thermal component of phonon broadening,  $\Gamma$ , has very similar  $T$  dependence in Figs.2(e) and 2(f), but the theory value is now smaller by about a factor of 2. What has not been probed experimentally is the signature of low energy

weight at  $\mathbf{q} \sim \mathbf{q}_{CE}$  at  $T \lesssim T_c$  - in manganites which show a thermally induced metal-insulator transition. This weight at  $\sim 10\%$  of the bare phonon scale is the key dynamical signature of short range correlated large amplitude distortions. Unless ionic disorder pins polarons, this low energy feature should be visible.

**Conclusions:** We have presented the first results on the coupled anharmonic dynamics of phonons and spins that emerges with increasing temperature in the Holstein-double exchange model. Past the low temperature harmonic window, we observe the expected nonlinearities attributable to ‘phonon-phonon’ and ‘magnon-magnon’ interactions. Beyond this, however, we see a striking ‘two peak’ structure in the momentum resolved phonon spectrum, involving: (i) low energy weight at  $\omega \ll \Omega$ , for  $\mathbf{q} \sim (\pi, \pi)$ , from slow tunneling of thermally generated spatially correlated polarons, and (ii) enhanced damping of the high energy,  $\omega \sim \Omega$ , feature due to scattering from magnetic fluctuations. The magnetic dynamics itself remains mostly insensitive to the phonon effects and can be described by a Heisenberg model. Our ‘high energy’ phonon trends compare well with inelastic neutron scattering in the manganites, although numerical values differ, and the low energy features should be visible in the low disorder samples at  $T \gtrsim 0.5T_{FM}$ .

- 
- [1] E. Dagotto, Science **309**, 257 (2005).
  - [2] Y. Tokura, *Colossal Magnetoresistive Oxides*, CRC Press (2000).
  - [3] *Handbook on the Physics and Chemistry of Rare Earths*, edited by K.A.Jr. Gschneidner, L. Eyring, M.B. Maple, North Holland (2000), Vols.30-31.
  - [4] S.W. Lovesey ed., *Dynamics of Solids and Liquids by Neutron Scattering*, Springer (1977).
  - [5] G.L. Squires, *Introduction to the Theory of Thermal Neutron Scattering*, 3rd Edition, Cambridge University Press (2012).
  - [6] M. Maschek, D. Lamago, J.-P. Castellán, A. Bosak, D. Reznik, and F. Weber, Phys. Rev. B **93**, 045112 (2016).
  - [7] M. Maschek, J.-P. Castellán, D. Lamago, D. Reznik, and F. Weber, Phys. Rev. B **97**, 245139 (2018).
  - [8] F. Weber, N. Aliouane, H. Zheng, J.F. Mitchell, D.N. Argyriou, and D.Reznik, Nature Materials **8**, 798 (2009).
  - [9] F. Weber, S. Rosenkranz, J.-P. Castellán, R. Osborn, H. Zheng, J.F. Mitchell, Y. Chen, Songxue Chi, J. W. Lynn, and D. Reznik, Phys. Rev. Lett. **107**, 207202 (2011).
  - [10] H. Miao, D. Ishikawa, R.Heid, M. Le Tacon, G. Fabbri, D. Meyers, G.D. Gu, A.Q.R. Baron and M.P.M. Dean, Phys. Rev. X **8**, 011008 (2018).
  - [11] R. Kajimoto, M. Fujita, K. Nakajima, K. Ikeuchi, Y. Inamura, M. Nakamura and T. Imasoto, Journal of Physics, Conference Series **502** 012056 (2014).
  - [12] Pengcheng Dai, H. Y. Hwang, Jiandi Zhang, J. A. Fernandez-Baca, S.-W. Cheng, C. Kloc, Y. Tomioka, and Y. Tokura, Phys. Rev. B **61**, 9553 (2000).
  - [13] J. Zhang, F. Ye, Hao Sha, P. Dai, J. A. Fernandez-Baca and E. W. Plummer, J. Phys.: Condens. Matter **19** 315204 (2007).
  - [14] Tapan Chatterji, F. Demmel, G. Dhalenne, M.-A. Drouin, A. Revcolevschi, and R. Suryanarayanan, Phys. Rev. B **72**, 014439 (2005).
  - [15] F. Ye, Pengcheng Dai, J. A. Fernandez-Baca, D. T. Adroja, T. G. Perring, Y. Tomioka, and Y. Tokura, Phys. Rev. B **75**, 144408 (2007).
  - [16] F. Moussa, M. Hennion, P. Kober-Lehoelleur, D. Reznik, S. Petit, H. Moudden, A. Ivanov, Ya. M. Mukovskii, R. Privezenstev, and F. Albenque-Rullier, Phys. Rev. B **76**, 064403 (2007).
  - [17] H. Ulbrich, F. Krüger, A. A. Nugroho, D. Lamago, Y. Sidis, and M. Braden, Phys. Rev. B **84**, 094453 (2011).
  - [18] Joel S. Helton, Susumu K. Jones, Daniel Parshall, Matthew B. Stone, Dmitry A. Shulyatev, and Jeffrey W. Lynn, Phys. Rev. B **96**, 104417 (2017).
  - [19] Superconductivity Of Metals And Alloys, P. G. de Gennes, Westview Press (1999).
  - [20] P. C. Hohenberg and B. I. Halperin, Rev. Mod. Phys. **49**, 435 (1977).
  - [21] B. J. Alder and T. E. Wainwright, J. Chem. Phys. **31**, 459 (1959).
  - [22] *Molecular Dynamics From Classical to Quantum Methods* edited by Perla B. Balbuena and Jorge M. Seminario, Elsevier (1999), *The Art of Molecular Dynamics Simulation*, D. C. Rapaport, Cambridge University Press (2004).
  - [23] A.J. Millis, P.B. Littlewood and B.I. Shraiman, Phys. Rev. Lett. **74**, 5144 (1995).
  - [24] A. Urushibara, Y. Morimoto, T. Arima, A. Asamitsu, G. Kido, and Y. Tokura, Phys. Rev. B **51**, 14103 (1995).
  - [25] Y. Okimoto, T. Katsufuji, T. Ishikawa, A. Urushibara, T. Arima, and Y. Tokura, Phys. Rev. Lett. **75**, 109 (1995).
  - [26] D. Akahoshi, M. Uchida, Y. Tomioka, T. Arima, Y. Matsui, and Y. Tokura, Phys. Rev. Lett. **90**, 177203 (2003).
  - [27] M. Uehara, S. Mori, C. H. Chen, and S.-W. Cheong, Nature, **399**, 560 (1999), M. Fäth, S. Freisem, A. A. Menovsky, Y. Tomioka, J. Aarts, J. A. Mydosh, Science, **285**, 1540 (1999).
  - [28] G. L. Liu, J.-S. Zhou, and J. B. Goodenough, Phys. Rev. B **70**, 224421 (2004).
  - [29] J. M. D. Coey, M. Viret, L. Ranno, and K. Ounadjela, Phys. Rev. Lett. **75**, 3910 (1995).
  - [30] E. Saitoh, Y. Okimoto, Y. Tomioka, T. Katsufuji, and Y. Tokura, Phys. Rev. B **60**, 10362 (1999).
  - [31] Adriana Moreo, Mathhias Mayr, Adrian Feiguin, Seiji Yunoki, and Elbio Dagotto, Phys. Rev. Lett. **84**, 5568 (2000).
  - [32] Yukitoshi Motome, Nobuo Furukawa, and Naoto Nagaosa, Phys. Rev. Lett. **91**, 167204 (2003).
  - [33] S. Kumar and P. Majumdar, Phys. Rev. Lett. **96**, 016602 (2006).
  - [34] Gia-Wei Chern, Kipton Barros, Zhentao Wang, Hidemaro Suwa, and Cristian D. Batista, Phys. Rev. B **97**, 035120 (2018).
  - [35] S. Bhattacharyya, S. S. Bakshi, S. Kadge, and P. Majumdar, Phys. Rev. B **99**, 165150 (2019).
  - [36] There is no genuine ferro to para transition in an  $O(3)$  model in 2D. However, the correlation length grows exponentially as  $T$  is reduced below the effective exchange scale,  $J_{eff}$ , and in any finite size calculation it is difficult to distinguish a merely long range ‘correlated’ state from a genuinely ordered one.
  - [37] William Fuller Brown, Jr., Phys. Rev. **130**, 1677 (1963).
  - [38] P. E. Kloeden and E. Platen, *Numerical Solution of Stochastic Differential Equations*, Springer, Berlin (1992).
  - [39] Pui-Wai Ma, S. L. Dudarev, Phys. Rev. B **83**, 134418 (2011).
  - [40] R. E. Watson, M. Blume, and G. H. Vineyard, Phys. Rev. **181**, 811 (1969).
  - [41] Minoru Takahashi, J. Phys. Soc. Jpn. **52**, 3592 (1983).
  - [42] The quantitative discrepancy between our results and experiments may arise partly from the use of acoustic phonons in the experiments, although these phonons had the same  $\Sigma_3$  symmetry as JT displacements.

# Supplemental Material for “Strongly anharmonic collective modes in a coupled electron-phonon-spin problem”

Sauri Bhattacharyya<sup>1</sup>, Sankha Subhra Bakshi<sup>1</sup>, Saurabh Pradhan<sup>2</sup> and Pinaki Majumdar<sup>1</sup>

<sup>1</sup> Harish-Chandra Research Institute, HBNI, Chhatnag Road, Jhansi, Allahabad 211 019, India

<sup>2</sup> Department of Physics and Astronomy, Uppsala University, 751 05 Uppsala, Sweden

(Dated: December 18, 2019)

We first discuss the derivation of the respective Langevin equations for phonons and spins. Next, the consistency between the results obtained using the present scheme and exact diagonalization based Monte Carlo is shown. Then, to hint at the various thermal regimes in phonons, the distribution of displacement and density fields are featured. A comparison of spectra in the present model with that obtained from a pure Holstein and a pure double exchange model are depicted afterwards. This elucidates the role of magnon-phonon coupling. Finally, real-time trajectories of phonon and spin fields are exhibited to create an insight into the detailed results.

## DERIVING THE LANGEVIN EQUATION

We reproduce the evolution equation below for reference

$$\begin{aligned} M \frac{d^2 x_i}{dt} &= -D_{ph} \frac{dx_i}{dt} - K x_i - \frac{\partial \langle H_{el} \rangle}{\partial x_i} + \xi_i(t) \\ \frac{d \vec{S}_i}{dt} &= -\vec{S}_i \times \left( \frac{\partial \langle H_{el} \rangle}{\partial \vec{S}_i} + \vec{h}_i \right) + D_s \vec{S}_i \times (\vec{S}_i \times \frac{\partial \langle H_{el} \rangle}{\partial \vec{S}_i}) \\ H_{el} &= \sum_{ij} (t_{ij} - \mu \delta_{ij}) \gamma_i^\dagger \gamma_j - g \sum_i n_i x_i \\ t_{ij}/t &= \sqrt{(1 + \vec{S}_i \cdot \vec{S}_j)/2} \end{aligned}$$

In what follows we comment on (i) the origin of the phonon and spin equations, (ii) the ‘noise’,  $\xi_i(t)$  and  $\vec{h}_i(t)$ , (iii) the choice of the damping parameters  $D_{ph}$  and  $D_s$ , and (iv) the robustness of the ‘equal time’ properties (at equilibrium) to variation in the damping parameters.

## Phonon equation

The derivation of the phonon equation of motion has been outlined before [2] in case of the pure Holstein model, which is in turn motivated by earlier work [3]. To quickly recapitulate, (i) A real time path integral is set up in the Keldysh formalism in terms of coherent state fields corresponding to  $x_i$  and  $c_i$  operators. (ii) Integrating out the quadratic electrons we obtain an effective action for the phonon fields on the Keldysh contour. (iii) We transform to ‘classical’ and ‘quantum’ variables, the average and difference of phonon fields on the forward and backward branches of the Keldysh contour, and expand the action perturbatively in the ‘quantum’ fields, assuming that the phonon timescale,  $\Omega^{-1}$ , is much larger than

the electronic timescale,  $t^{-1}$  ( $t$  is the hopping). (iv) Integrating out the ‘quantum’ fields at Gaussian level leads to a stochastic equation of motion for the ‘classical’ fields.

The main difference here with respect to the pure Holstein model is the (time dependent) modulation of the hopping amplitude,  $t_{ij}$ , due to fluctuation in the orientation of the spins. The implicit dependence of the ‘force’ term  $\frac{\partial \langle H_{el} \rangle}{\partial x_i} = g n_i(t)$  on the spin configuration is relatively weak.

## Spin equation

The spin equation is written based on arguments presented in Ref.4. The significance of the different terms is as follows: (i) The torque term describes semiclassical dynamics of the fixed magnitude moments in an effective magnetic field. In our case, this field is computed as a gradient of the instantaneous electronic energy with respect to the local spin  $\vec{S}_i$ . (ii) The dissipation is proportional to the angular momentum of the moments, in analogy with the motion of ions. When the dynamics is restricted to the surface of a unit sphere, our LLGB equation emerges.

There are alternate derivations starting from a model of local moments coupled to phonons [5] and/or conduction electrons [6, 7] and then employing the Keldysh formalism. One makes similar assumptions there as in the electron-phonon case, namely that the moments are ‘slow’ compared to other microscopic degrees of freedom and that the electronic density of states is gapless and conforms to the Ohmic dissipation model.

The spin equation differs from that for the double exchange model only in the implicit dependence of bond kinetic energy average  $\langle \gamma_i^\dagger \gamma_j \rangle$  on the phonon field. It differs from the Heisenberg model, additionally, via the factor  $1/\sqrt{(1 + \vec{S}_i \cdot \vec{S}_j)/2}$ , which modifies the local field acting on the site  $i$ .

## Specifying the noise

The ‘noise’ which drives the phonon field has a correlator

$$\langle \xi_i(t) \xi_j(t') \rangle = g^2 \Pi_{ij}(t, t')$$

where  $\Pi$  is the Keldysh component of the electronic polarizability, in the background  $x_i(t)$ . On the assumption that we are at ‘high temperature’,  $\Omega \ll k_B T$ , and that the electronic density of states is gapless, we obtain the Langevin form used



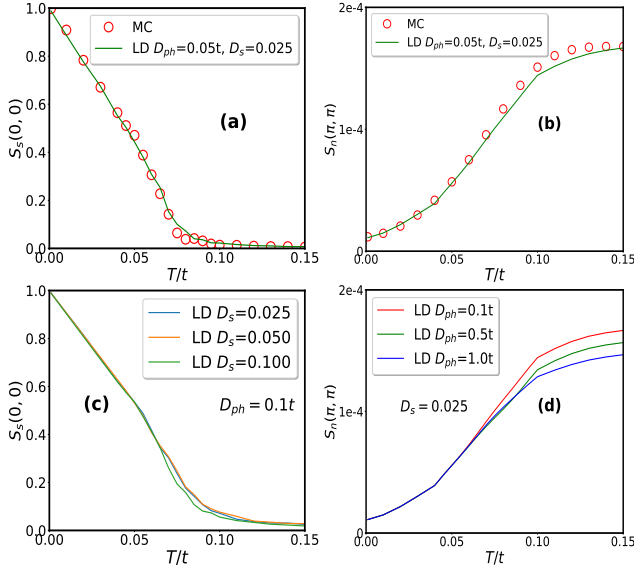


FIG. 1. (a)-(b): Comparison of Langevin results with Monte Carlo. (a) The ferromagnetic feature  $S_s(0,0)$  in the magnetic structure factor and (b) the Fourier transform of the density-density correlation  $S_n$  at  $\mathbf{q} = (\pi, \pi)$ . There is a very good agreement for the chosen  $D_s$  and  $D_{ph}$  values. (c) The dependence of  $S_s(0,0)$  on  $D_s$  for three values  $D_s = 0.025, 0.05, 0.1$ , and (d) of  $S_n(\pi, \pi)$  on  $D_{ph}$  for three values  $D_{ph} = 0.1t, 0.5t, 1.0t$ . In both cases, we see an insensitivity to dissipation rates.

in the paper. Although we use the high temperature approximation throughout to simplify the noise correlator, the essential dynamical features of the phonons are retained even for  $k_B T \lesssim \Omega$  through the ‘electronic force’ term.

The spin noise  $\tilde{h}_i$  is chosen to be Markovian, obeying the fluctuation-dissipation theorem, for simplicity. In an actual derivation from a Keldysh action, the noise correlator is proportional to the Keldysh spin polarizability  $[\Pi_{ij}^S(t, t')]^{\mu\nu}$ , that has a natural frequency scale  $\sim t$ . For low frequencies ( $\omega \ll t$ ) and high temperatures ( $\omega \ll k_B T$ ), the present Markovian form may be used. Once again, we apply this approximation at all temperatures, assuming that the key dynamical features are captured through the ‘electronic torque’ term.

### The damping parameters

Microscopically, in the Holstein double exchange model, the phonons couple to the local density and the moments to the local conduction electron spin. Hence, the dissipation channels arise from particle-hole excitations in the charge and spin sectors. These involve the charge and spin susceptibilities of the parent electronic system. At low temperature one may approximate these by their ‘bare’ versions. The dissipation rates  $D_s$  and  $D_{ph}$  arise from the imaginary parts of the ‘linear’, low-frequency part of these functions.  $D_{ph}$  carries a prefactor of  $g^2$ , while  $D_s$  is proportional to  $t^2$ . An actual calculation

reveals that  $D_s \sim 0.1t$  and  $D_s \sim 0.1$  at low temperatures.

### CONSISTENCY BETWEEN LANGEVIN DYNAMICS AND MONTE CARLO

The ‘static’ physics at equilibrium for the Holstein-double exchange model can be extracted from an exact diagonalisation based Monte Carlo (ED-MC), when we assume the phonons and spins to be classical. That assumes  $M \rightarrow \infty$ , *i.e.*,  $\Omega \rightarrow 0$ , and the ‘size’ of the spin  $S \rightarrow \infty$  (to be absorbed in the Hund’s coupling). In that case the probability for a phonon-spin configuration is:

$$P\{x, S\} \propto \text{Tr} e^{-\beta(H_{el} + H_{stiff})}$$

$$H_{el} = \sum_{ij} (t_{ij} - \mu \delta_{ij}) \gamma_i^\dagger \gamma_j - g \sum_i n_i x_i$$

$$t_{ij}/t = \sqrt{(1 + \vec{S}_i \cdot \vec{S}_j)/2}$$

$$H_{stiff} = \frac{1}{2} K \sum_i x_i^2$$

The trace over the electrons can be performed numerically by diagonalising  $H_{el}$ . This forms the heart of ED based MC and yields results that do not have the effect of the parameters  $M$ ,  $D_{ph}$ ,  $D_s$  that enter the Langevin equation. It is important to verify that the Langevin approach, with its additional dissipative parameters, yields equilibrium results that are consistent with MC.

In Fig.1, we show the behaviour of the spin structure factor  $S_s(\mathbf{q})$  and the density structure factor  $S_n(\mathbf{q})$  at  $\mathbf{q} = (0, 0)$  and  $(\pi, \pi)$  respectively.

$$S_s(\mathbf{q}) = \frac{1}{N^2} \sum_{ij} \vec{S}_i \cdot \vec{S}_j e^{i\mathbf{q} \cdot (\vec{r}_i - \vec{r}_j)}$$

$$S_n(\mathbf{q}) = \frac{1}{N^2} \sum_{ij} \langle n_i \rangle \langle n_j \rangle e^{i\mathbf{q} \cdot (\vec{r}_i - \vec{r}_j)}$$

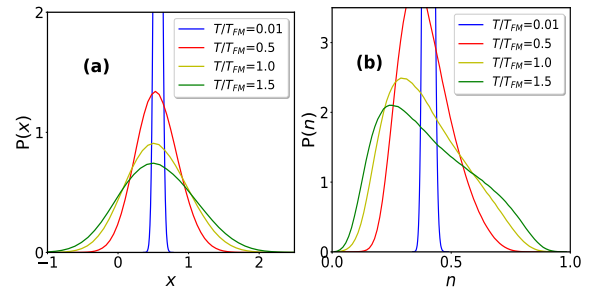


FIG. 2. (a)-(b): The distribution of distortions ( $P(x)$ ) and density ( $P(n)$ ) for four temperatures-  $T/T_{FM} = 0.01, 0.5, 1.0, 1.5$ . The former broadens gradually on heating up. The latter shows a more interesting evolution from a sharp unimodal profile ( $T \ll T_{FM}$ ) through a positively skewed, long tailed distribution (near  $T_{FM}$ ) to finally a plateau-like structure beyond  $T_{FM}$ . The quick onset of anharmonicity, presence of large distortions near  $T_{FM}$ , and the merging of large oscillations with polarons at high  $T$ , are all hinted at.

We test out different  $D_s$  and  $D_{ph}$  values. In the top panel, the results on these obtained using the two methods (Langevin dynamics and Monte Carlo annealing) are shown. The match is remarkable. For both the spin and density cases, the bottom panel shows an insensitivity of the Langevin inferred structure factor to the damping rates  $D_{ph}$  and  $D_s$ .

### DISTRIBUTION OF DISPLACEMENT AND DENSITY

In Fig.2, we show the distribution of displacements ( $P(x, T)$ ) and electron density  $P(n, T)$  in four temperature regimes. The low temperature state is uniform and has a sharp, unimodal profile for both of them. The former shows gradual broadening thereafter, not underscoring the thermal polaron formation. However, the density distribution broadens

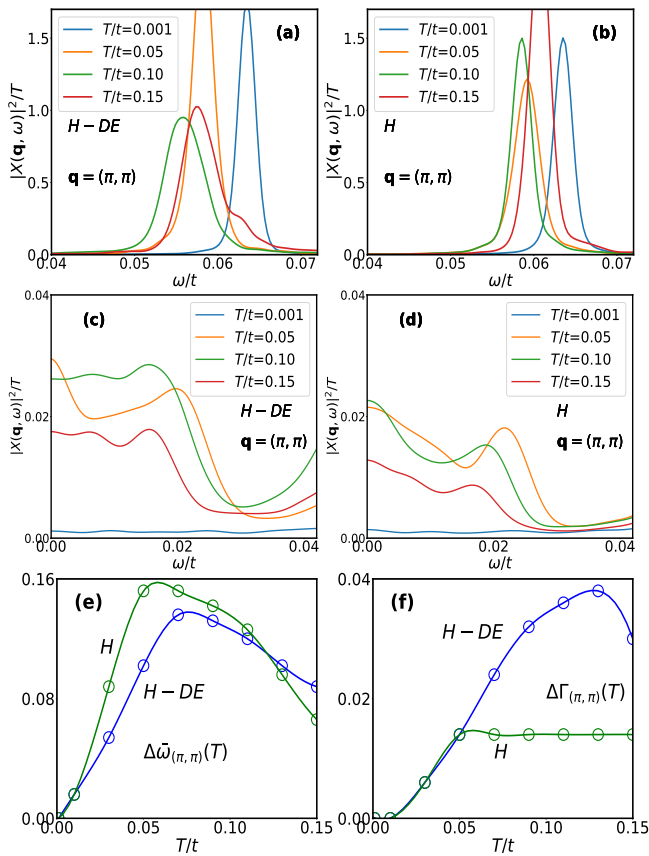


FIG. 3. (a)-(b): Comparison of ‘high energy’ part of phonon lineshapes at  $\mathbf{q} = (\pi, \pi)$  for different temperature regimes between the present model (H-DE) and a pure Holstein model (H) at comparable density. (c)-(d): Same for ‘low energy’ part of the spectra. Similar qualitative features are seen in both cases, but the effects are stronger in the former. (e): The extracted softening  $\Delta\tilde{\omega}_{(\pi, \pi)}(T)$  compared between the H-DE and Holstein models. The results are broadly similar. (f): The linewidth  $\Delta\Gamma_{(\pi, \pi)}(T)$  compared between the H-DE and Holstein models. In the Holstein model the width saturates at some temperature, without the peak that one observes in the H-DE model. The larger H-DE damping and the peak feature in  $T$  dependence arise due to the magnetic degrees of freedom.

quickly ( $T/T_{FM} = 0.5$ ), signifying the onset of highly anharmonic behaviour. Near  $T_{FM}$ , a left-skewed, long-tailed shape is seen, which depicts thermally induced polarons. Finally, beyond  $T_{FM}$ , a broad, plateau-like structure emerges, hinting at the merging of distortions of different sizes.

### PHONON SPECTRA IN THE HOLSTEIN-DOUBLE EXCHANGE AND HOLSTEIN MODELS

In Fig.3 we first compare lineshapes in four temperature regimes between the Holstein-double exchange (H-DE) and the Holstein (H) model at comparable density. (a) and (b) feature the ‘high energy’ spectra. The basic trends are similar. However, the extent of softening and broadening close to  $T_{FM}$  in the former is much more accentuated compared to the Holstein model for the same temperature. The basic reason is the presence of increasing spin disorder in the former which effectively reduces the electronic bandwidth and enhances the

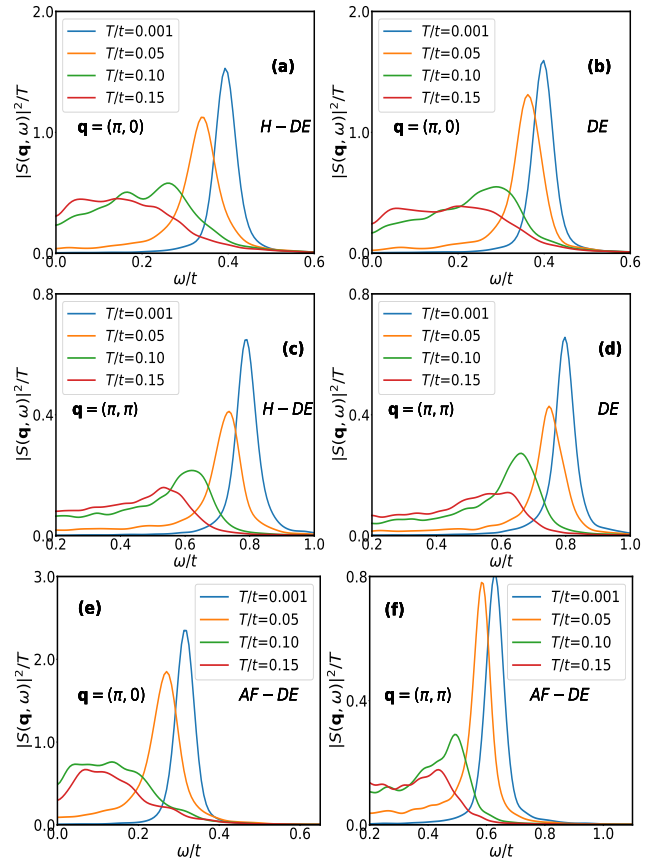


FIG. 4. (a)-(b): Comparison of magnon lineshapes at  $\mathbf{q} = (\pi, 0)$  for different temperature regimes between the present model and a pure double exchange model at comparable density. (c)-(d): Same for  $\mathbf{q} = (\pi, \pi)$ . One observes a qualitative similarity in all regimes, signifying the subdued effect of magnon-phonon coupling on magnons. (e)-(f): Magnon spectra at the same wavevectors for a DE model with small ( $J_{AF} = 0.2J_{eff}$ ) AF coupling. We observe a bandwidth shortening at low  $T$  and smaller dampings compared to the former.



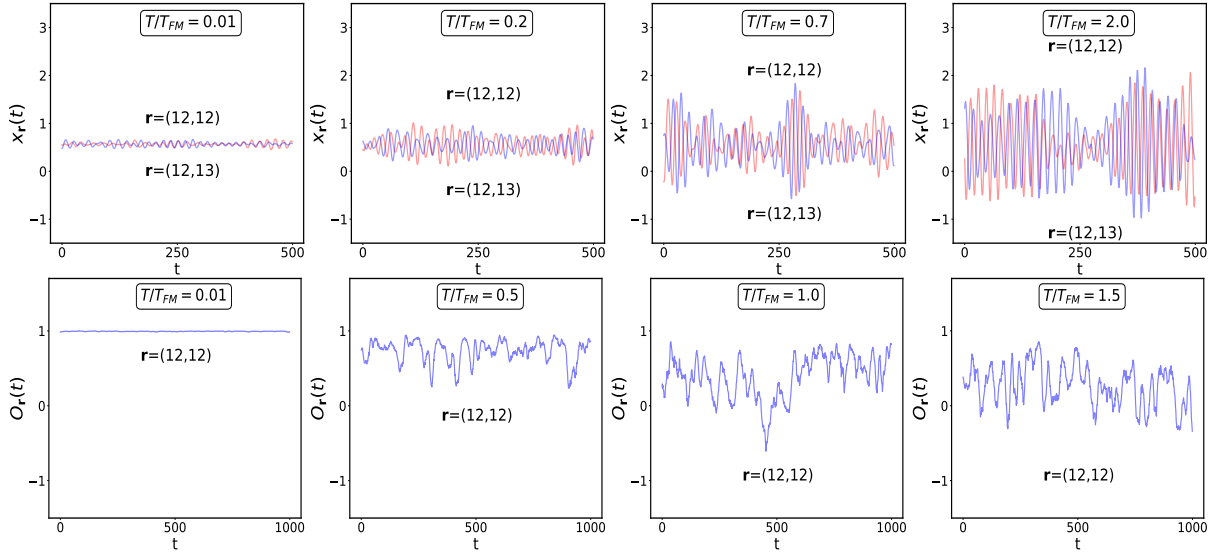


FIG. 5. Top panel: Real-time trajectories of  $x_i(t)$  on the central site at four temperatures-  $T/T_{FM} = 0.01, 0.5, 1.0, 1.5$ . One observes a gradual increase in the amplitude of oscillations on heating up. The ‘flip’ moves, involving large ( $\sim O(g/K)$ ) changes in  $x_i$ , are merged with large oscillations near  $T_{FM}$ . They first start showing up near  $\sim 0.7T_{FM}$ . Bottom: Trajectories of the magnetic overlap function  $O_i(t)$  on the same site. Here, a proliferation of ‘sign changes’ are seen with a large period close to criticality.

effective coupling to phonons. However, we comment that the quantitative increase in damping is underestimated by just considering this effect, which hints at a crucial role of spatial correlations. The middle panel ((c) and (d)) exhibits the thermal evolution of low-frequency weight, which is again sharper in the H-DE case, due to well-formed polarons and their associated tunneling. In the bottom panel ((e) and (f)), the softenings and linewidths extracted from the corresponding line-shapes are shown ((c) and (d)). We see a more detailed thermal comparison here, which corroborates the above findings. The main result is a gradual and substantial rise in phonon damping near  $T_{FM}$  in the present model, which is absent in the pure Holstein case, where damping saturates by  $0.5T_{FM}$ . Moreover, the rise in softening is sharper in the pure Holstein case.

### MAGNON SPECTRA IN THE HOLSTEIN-DOUBLE EXCHANGE AND DOUBLE EXCHANGE MODELS

Fig.4 highlights the comparison of magnon spectrum for the H-DE model with that of the DE model. The top and middle panels feature lineshapes at  $\mathbf{q} = (\pi, 0)$  and  $\mathbf{q} = (\pi, \pi)$  respectively. The qualitative features remain the same, which confirms that the effects of magnon-phonon coupling on the spin dynamics are weak. Moreover, the double-exchange model spectra are qualitatively similar to those of a nearest-neighbour Heisenberg model with  $J_{eff} \sim 0.1t$ . This means that the magnon dynamics is fairly conventional. In the bottom panel ((e) and (f)), we show lineshapes at the same wavevectors for a DE model with a small ( $J_{AF} = 0.2J_{eff}$ ) AF coupling, which is realistic from the materials point of

view. The main result is a smaller low  $T$  bandwidth and finite temperature linewidths limited by this scale. The  $T_{FM}$  in this case is  $\sim 0.08t$ .

### REAL TIME TRAJECTORIES

In Fig.5, we depict the representative real time trajectories from which we obtain the phonon and magnon power spectrum. The top row shows  $x_i(t)$  while the lower row shows the magnetic overlap function:

$$O_i(t) = \frac{1}{4} \sum_{\delta} \vec{S}_i(t) \cdot \vec{S}_{i+\delta}(t)$$

where  $\delta$  are the four neighbours of site  $i$ . We show results in four temperature regimes- harmonic, anharmonic, polaronic and high for phonons and low, intermediate, critical and high for magnons. The chosen site is located at the middle of the system. The top panel also follows its right neighbour.

In the harmonic regime, the phonon dynamics is saturated by small oscillations about a homogeneous state. Anharmonic behaviour sets in quickly ( $T \sim 0.2T_{FM}$ ), where oscillations of larger amplitude ( $> 10\%$  of mean value) prevail and effect of mode coupling shows up in  $\Gamma_{ph}(\mathbf{q})$ . Next comes the polaronic regime ( $T/T_{FM} = 0.7$ ), where short-range correlated ‘burst’ like events coexist with anharmonic oscillations. These lead to the remarkable low-frequency weight transfer. Finally, well beyond  $T_{FM}$ , distortions of several scales get merged together and short-range correlations weaken.

The magnetic overlap  $O_i(t)$  is perfect at low  $T$ , but shows a gradual proliferation of ‘sign changing’ moves on heating, which eventually kill the ferromagnetic order.

- 
- [1] Sanjeev Kumar and Pinaki Majumdar, Phys. Rev. Lett. **96**, 016602 (2006).
- [2] S. Bhattacharyya, S. S. Bakshi, S. Kadge, and P. Majumdar, Phys. Rev. B **99**, 165150 (2019).
- [3] D. Mozyrsky, M.B. Hastings, and I. Martin, Phys. Rev. B **73**, 035104 (2006).
- [4] Pui-Wai Ma, S. L. Dudarev, Phys. Rev. B **86**, 054416 (2012).
- [5] A. Rebei and G. J. Parker, Phys. Rev. B **67**, 104434 (2003).
- [6] A. Rebei, W. N. G. Hitchon, and G. J. Parker, Phys. Rev. B **72**, 064408 (2005).
- [7] B. Mera, V. R. Vieira, and V. K. Dugaev, Phys. Rev. B **88**, 184419 (2013).